Crystal and magnetic structures of $RbMnF_4$ and $KMnF_4$ investigated by neutron powder diffraction: the relationship between structure and magnetic properties in the Mn^{3+} layered perovskites $AMnF_4$ (A=Na, K, Rb, Cs)

1993 J. Phys.: Condens. Matter 5 4909

(http://iopscience.iop.org/0953-8984/5/28/007)

J. Phys.: Condens. Matter 5 (1993) 4909–4928. Printed in the UK

Crystal and magnetic structures of $RbMnF_4$ and $KMnF_4$ investigated by neutron powder diffraction: the relationship between structure and magnetic properties in the Mn^{3+} layered perovskites $AMnF_4$ (A = Na, K, Rb, Cs)

M C Morón†, F Palacio† and J Rodríguez-Carvajal‡

† Instituto de Ciencia de Materiales de Aragón, CSIC-Universidad de Zaragoza, E-50 009 Zaragoza, Spain

‡ Institut Laue–Langevin, BP 156X, F-38 042 Grenoble, France

Received 22 September 1992, in final form 25 January 1993

Abstract. The crystal and magnetic structures of $RbMnF_4$ and $KMnF_4$ have been determined by neutron powder diffraction. The crystal symmetry of both compounds belongs to the layered perovskite structure and exhibits a pseudo-tetragonal unit cell, space group $P2_1/a$. The $[MnF_2F_{4/2}]^-$ octahedra show a distortion induced by both steric and Jahn–Teller effects. They are also tilted by an angle which depends on the size of the alkali ion. $KMnF_4$ orders as a non-collinear antiferromagnet below 5.2 ± 0.1 K exhibiting four magnetic sublattices with an angle between the two spin directions of 17°. $RbMnF_4$ is a collinear antiferromagnet below 3.7 ± 0.1 K. Interestingly enough and contrary to what is found for the K compound, there are two active irreducible representations in the magnetic structure of the Rb derivative. Moreover, the relationship between crystal structure and magnetic behaviour has been investigated in the $AMnF_4$ (A = Na, K, Rb, Cs) series. The sign of the isotropic magnetic interaction is studied as a function of the superexchange angle Mn–F–Mn and the degree of distortion of the octahedra. The critical superexchange angle α_c, at which the *crossover* between ferromagnetic ($\alpha > \alpha_c$) and antiferromagnetic ($\alpha < \alpha_c$) isotropic interaction takes place in the $AMnF_4$ family, is found to be $\alpha_c \simeq 147°$.

1. Introduction

Fluorinated Mn^{3+} derivatives provide a rich variety of low-dimensional magnetic systems with appealing properties, both magnetic and structural. Several series of structurally related compounds can be formed where the magnetic properties show small, although significant, differences between the members of the series, thus affording families with quasi-ideal conditions for the study of magneto-structural correlations (Pebler *et al* 1987, Palacio *et al* 1988). An important characteristic of these Mn^{3+} compounds is the presence of strong Jahn–Teller distortions which severely affects their structures and magnetism.

From a structural point of view, the compounds of general formula AMF_4, where M refers to a first-row transition metal and A to an alkali ion, tend to form layers of corner-sharing $[MF_2F_{4/2}]^-$ octahedra separated by the alkali ions, their structure being of the $TlAlF_4$ type (Aleksandrov *et al* 1987). Thus, $CsMnF_4$ was found to crystallize in the space group $P4/nmm$ (Massa and Steiner 1980) while $NaMnF_4$ and $LiMnF_4$ have been described as isomorphic in the space group $P2_1/c$ (Molinier *et al* 1991, Wandner and Hoppe 1987). The crystal structures of the $CsMnF_4$, $NaMnF_4$ and $LiMnF_4$ compounds belong to the well

0953-8984/93/284909+20$07.50

known layered-perovskite family and therefore they are largely influenced by the steric effect of the alkali ion.

On the other hand, the magnetic behaviour of the $AMnF_4$ compounds also depends very strongly on the size of the alkali ion. Thus, susceptibility measurements on powder samples show that for A = Cs the compound orders as a ferromagnet at 21 K while for A = K, Rb, NH_4 the corresponding derivatives order as antiferromagnets at, respectively, 6 K, < 4.5 K and 10 K (Köhler *et al* 1978). Moreover, neutron powder diffraction experiments have confirmed the ferromagnetic ordering in $CsMnF_4$ (Massa and Steiner 1980) while they suggest a non-collinear antiferromagnetic structure in $NaMnF_4$ below 13.0±0.5 K (Molinier *et al* 1991). The magnetic properties of $LiMnF_4$ have not been reported up to now. Such a diversity in the magnetic behaviour opens several interesting questions whose answer demands a detailed investigation of the magneto-structural correlations in these compounds. The $AMnF_4$ (A = Na, K, Rb, Cs) series is especially suitable for this type of study since the layered-perovskite structure constitutes a rather simple arrangement of atoms.

In order to understand the magnetic properties of a given compound an accurate knowledge of the corresponding crystal structure in the ordered phase is required. Particularly, a precise localization of the fluorine atoms is important in this type of layered perovskite compounds due to the different tilting schemes that the $[MF_2F_{4/2}]^-$ octahedra may exhibit (Aleksandrov *et al* 1987). For this purpose, neutrons are more suitable than x-rays.

In this work we report the crystal and magnetic structures of $RbMnF_4$ and $KMnF_4$ studied by neutron powder diffraction. The magnetic structures of both compounds are studied in the frame of Bertaut's macroscopic theory (Bertaut 1968). The value of the magnetic moment of each sublattice as a function of the temperature is determined for $RbMnF_4$ and $KMnF_4$, resulting in finding the corresponding critical temperatures. Finally, the influence of the crystal structure in the magnetic properties of the $AMnF_4$ series is discussed. Throughout this work, we have adopted the convention of taking the c axis perpendicular to the MnF_4 layers.

2. Experimental details

Polycrystalline samples of $AMnF_4$ (A = K and Rb) were prepared by controlled dehydration of $AMnF_4 \cdot H_2O$ (A = K and Rb) at 120°C. The hydrated compounds were synthesized following previously described methods (Kaucic and Bukovec 1979, Palacio *et al* 1988). The samples were tested by x-ray powder diffraction in order to determine the presence of possible impurities. None were found.

The neutron scattering experiments were performed at the high-flux reactor of the Institut Laue–Langevin in Grenoble (France). Each sample was put into a cylindrical vanadium can ($d = 8$ mm, $h = 50$ mm) and inserted into a helium cryostat. The temperature was computer controlled and its stability during the measurements was better than 0.1 K.

In order to solve the crystal structures of both compounds, the high-resolution neutron powder diffractometer D2B ($\lambda \cong 1.594$ Å) was used in its high-flux mode of operation moving the detector bank in steps of 0.05° to cover a total angular range of $5° \leqslant 2\theta \leqslant 150°$. Diffraction patterns were collected for $KMnF_4$ at 291 and 19.1 K, and for $RbMnF_4$ at 288 and 9.6 K.

On the other hand, the high-flux medium-resolution neutron powder diffractometer D1B ($\lambda \cong 2.52$ Å) was chosen to study the magnetically ordered phase. The good resolution at small angles and the high neutron flux make D1B very suitable to follow the thermal

evolution of the magnetic reflections. Diffraction patterns were recorded between 1.5 and 9.4 K for $KMnF_4$ and between 1.5 and 4.8 K for $RbMnF_4$ in the angular range $8° \leqslant 2\theta \leqslant 88°$.

The data were analysed by using the program FULLPROF (Rodríguez-Carvajal 1990) which allows the Rietveld refinement of multiphase patterns combining nuclear and magnetic structures.

3. Analysis and results

3.1. Structural study of $RbMnF_4$ and $KMnF_4$

Due to the expected severe pseudo-symmetry of the unit cell of $RbMnF_4$, special care was taken to find the correct space group. The search for the starting unit cell parameters was performed by whole-profile matching without a structural model.

Several trials were performed. They were based on superstructures derived from the a_0 and c_0 unit cell parameters where a_0 and c_0 correspond to the ideal tetragonal structure of $TlAlF_4$ or aristotype (Aleksandrov *et al* 1987). Unit cells such as $\{a_0, a_0, c_0\}$, $\{\sqrt{2}a_0, \sqrt{2}a_0, c_0\}$ or $\{2a_0, a_0, c_0\}$ did not index the full pattern of $RbMnF_4$. The first reasonable agreement was obtained for a tetragonal cell $\{2a_0, 2a_0, c_0\}$ with $a \cong 7.77$ Å ($\cong 2a_0$) and $c \cong 6.04$ Å. Three tetragonal space groups $P4/m$ (No 83), $P4/mmm$ (No 123) and $P4/mbm$ (No 127) were comparable with the experimental reflection conditions. However, refinements of the $TlAlF_4$ structural model using these space groups did not give good agreement between the observed and calculated diffraction patterns.

Allowing a small orthorhombic distortion, a unit cell with $a = 7.8175(4)$ Å, $b = 7.7699(3)$ Å and $c = 6.0417(2)$ Å gave a satisfactory agreement between the observed and calculated profiles. The following space groups were found to be compatible with the unambiguous reflection conditions (hkl: no conditions; $00l$: no conditions; $hk0$: no conditions for h): $Pmmm$ (No 47), $Pbmb$ (No 49), $Pmmb$ (No 51), $Pbmm$ (No 51) $Pmam$ (No 51), $Pbab$ (No 54) $Pbam$ (No 55) and $Pmab$ (No 57). Only the space group $Pmab$ gave good results in the refinements. The crystal structure of $RbMnF_4$ was refined using 395 independent reflections and 28 refined parameters. The reliability factors, using background corrected counts, were $R_B = 6.6$, $R_P = 16.3$, $R_{WP} = 16.8$, $R_{EXP} = 9.5$ and $\chi^2 = 3.1$. In fact, in a preliminary work the structural arrangement of $RbMnF_4$ was described in this space group (Morón *et al* 1992). It is worth mentioning that $Pmab$ has been reported to be the space group of the room-temperature phase of the related compound $RbFeF_4$ (Morón *et al* 1990).

In spite of the good R factors some significant differences were found in some regions of the diffraction pattern suggesting a reduction in symmetry. Three monoclinic centrosymmetric subgroups of $Pmab$, namely $P2_1/m11$ (No 11), $P112/b$ (No 13) and $P12_1/a1$ (No 14), were checked. The best agreement was found for the space group $P2_1/a$ by using 732 independent reflections and 38 free parameters ($R_B = 6.0$, $R_P = 13.1$, $R_{WP} = 13.2$, $R_{EXP} = 9.6$ and $\chi^2 = 1.9$). The observed and calculated patterns are shown in figure 1.

As a result of this study, $RbMnF_4$ was found to crystallize at 288 K in the space group $P2_1/a$ with $a = 7.8119(4)$ Å, $b = 7.7761(4)$ Å, $c = 6.0469(3)$ Å, $\beta = 90.443(4)°$ and $Z = 4$. $P2_1/a$ was also found to be the space group at 9.6 K with $a = 7.7865(3)$ Å, $b = 7.7447(3)$ Å, $c = 5.9968(2)$ Å and $\beta = 90.434(3)°$ ($R_B = 5.1$, $R_P = 11.8$, $R_{WP} = 12.9$, $R_{EXP} = 7.1$ and $\chi^2 = 3.3$).

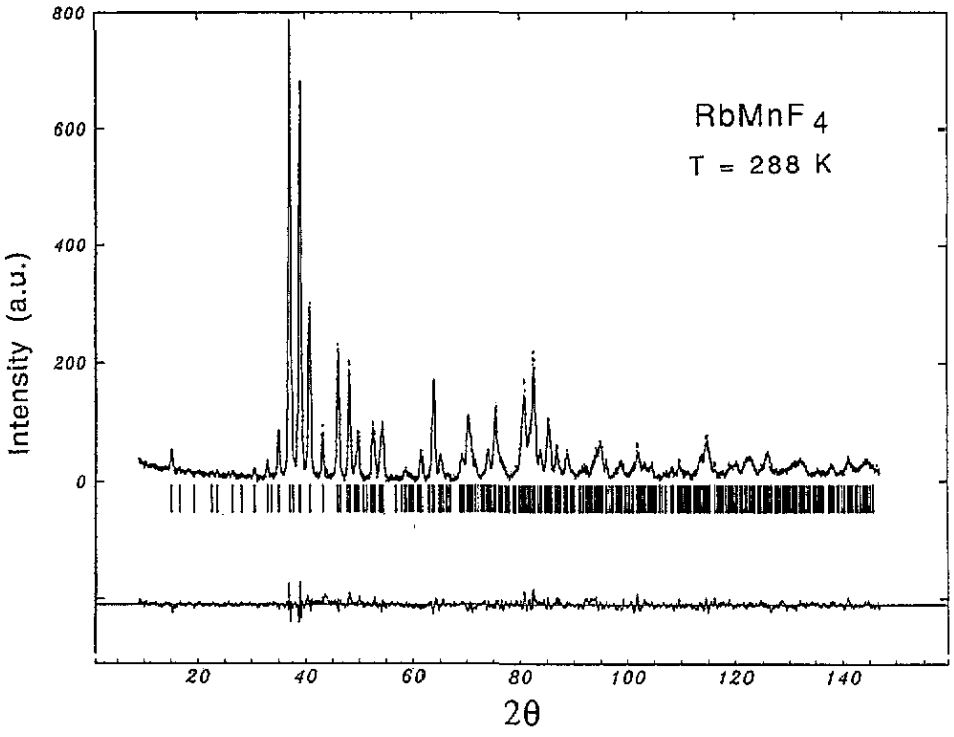

Figure 1. Observed (dotted curve) and calculated (full curve) intensities of $RbMnF_4$ at 288 K. The difference pattern $Y_{obs} - Y_{calc}$ is given at the bottom of the figure on the same scale. Angular positions of the allowed Bragg reflections are indicated by small bars.

The spatial arrangement of the atoms in $RbMnF_4$ consists of layers of $[MnF_2F_{4/2}]^-$ corner-sharing octahedra separated by Rb atoms (figure 2). The atomic coordinates are reported in table 1 while selected interatomic distances and angles are given in table 2. The octahedra exhibit a distortion induced by both steric and Jahn–Teller effects. This additional Jahn–Teller distortion could be responsible for the differences in symmetry when orthorhombic $RbFeF_4$ is compared with monoclinic $RbMnF_4$. The shortest Mn–F distance corresponds to the axial fluorine atoms being the long axis of the octahedra antiferrodistortively ordered within the layers (figure 3). The mean Mn–F distance is 1.95 Å, very close to the value of 1.92 Å predicted by the bond-valence sum (BVS) rule (Brese and O'Keeffe 1991, Brown and Altermat 1985).

Consecutive octahedra along [100] are tilted in phase around the *a* axis while those along [010] are tilted in anti-phase around the *b* axis (figure 3). In order to know the magnitude of such a tilt scheme, the tilt angles around the three crystallographic axes have been calculated and are given in table 3. No correction has been made to take into account the influence of the octahedra distortion in the tilt angles. Considering the same Mn atom and the same tilt axis, the difference observed in table 3 between the tilt angles calculated from different fluorine atoms is due to the distortion of the octahedra. This is the reason why the tilt angle around the *c* axis is zero, within the experimental error, when taken from F(1) but not negligible when taken from F(2). Table 3 also indicates that the relative tilting between octahedra centred on inequivalent Mn atoms is much larger along the *b* axis ($\cong 27°$ on average) than along the *a* axis ($\cong 1°$ on average).

Table 1. Atomic coordinates and thermal parameters for $RbMnF_4$ and $KMnF_4$. The two sets of values for each atom correspond to high (upper row) and low (lower row) temperatures. These are 288 and 9.6 K for the Rb and 291 and 19.1 K for the K compounds.

Atom	x	y	z	B (Å^2)
$RbMnF_4$				
Mn(a)	0	0	0	1.0(1)
	0	0	0	0.3(1)
Mn(c)	0	0.5	0	0.8(1)
	0	0.5	0	0.7(1)
F(1)	−0.0024(7)	0.2412(7)	0.0932(5)	1.51(6)
	−0.0003(5)	0.2409(5)	0.1001(4)	0.87(5)
F(2)	0.2587(6)	0.0152(3)	−0.0805(6)	2.29(6)
	0.2620(4)	0.0156(2)	−0.0834(8)	1.04(4)
F(3)	0.0450(4)	−0.0600(7)	0.2817(6)	1.37(7)
	0.0489(5)	−0.0616(6)	0.2833(4)	0.60(6)
F(4)	−0.0504(4)	0.5563(7)	0.2868(5)	1.48(7)
	−0.0528(3)	0.5600(6)	0.2854(4)	0.47(5)
Rb	0.7468(6)	0.2892(3)	0.4811(4)	1.94(5)
	0.7460(4)	0.2940(2)	0.4830(3)	0.51(3)
$KMnF_4$				
Mn(a)	0	0	0	1.12(7)
	0	0	0	0.30(5)
Mn(c)	0	0.5	0	1.25(7)
	0	0.5	0	0.65(6)
F(1)	0.0034(3)	0.2361(3)	0.1150(3)	2.02(4)
	0.0018(3)	0.2353(3)	0.1201(3)	0.85(2)
F(2)	0.2625(3)	0.0193(2)	−0.0948(3)	2.12(4)
	0.2625(2)	0.0209(2)	−0.0969(3)	0.75(3)
F(3)	0.0554(2)	−0.0761(3)	0.2884(3)	1.49(4)
	0.0562(2)	−0.0758(2)	0.2892(3)	0.67(3)
F(4)	−0.0641(2)	0.5614(3)	0.2883(4)	1.92(4)
	−0.0647(2)	0.5653(2)	0.2888(3)	0.58(3)
K	0.7458(6)	0.3024(3)	0.4886(4)	1.90(5)
	0.7465(4)	0.3050(2)	0.4870(3)	0.49(3)

The procedure used to find the space group for $RbMnF_4$ was also followed for $KMnF_4$. As a result, $KMnF_4$ was found to crystallize at 291 K in the space group $P2_1/a$ with $a = 7.7062(2)$ Å, $b = 7.6568(2)$ Å, $c = 5.7889(1)$ Å, $\beta = 90.432(2)°$ and $Z = 4$ ($R_B = 5.1$, $R_P = 11.6$, $R_{WP} = 11.6$, $R_{EXP} = 9.3$ and $\chi^2 = 1.6$) (Morón *et al* 1992). The difference between the calculated and observed patterns is shown in figure 4. As in the case of the Rb derivative, there is no structural phase transition between room and low temperature. $P2_1/a$ also remains the space group at 19.1 K with $a = 7.6830(1)$ Å,

Table 2. Main interatomic distances (Å) and angles (°) for $RbMnF_4$ and $KMnF_4$. The two sets of values for each atom correspond to high (upper row) and low (lower row) temperatures. These are 288 and 9.6 K for the Rb and 291 and 19.1 K for the K compounds.

Distances		Angles	
$RbMnF_4$			
Mn(a)–F(1)	1.959(5)	F(1)–Mn(a)–F(2)	91.4(2)
	1.960(4)		*91.2(1)*
Mn(a)–F(2)	2.086(5)	F(1)–Mn(a)–F(3)	91.3(2)
	2.108(3)		92.1(2)
Mn(a)–F(3)	1.798(4)	F(2)–Mn(a)–F(3)	93.0(2)
	1.802(3)		92.3(1)
Mn(c)–F(1)	2.090(5)	F(1)–Mn(c)–F(2)	90.1(2)
	2.094(4)		90.7(1)
Mn(c)–F(2)	1.947(5)	F(1)–Mn(c)–F(4)	91.6(2)
	1.920(3)		91.5(2)
Mn(c)–F(4)	1.834(4)	F(2)–Mn(c)–F(4)	92.1(2)
	1.824(3)		92.1(1)
$KMnF_4$			
Mn(a)–F(1)	1.926(2)	F(1)–Mn(a)–F(2)	90.8(1)
	1.923(2)		91.1(1)
Mn(a)–F(2)	2.105(2)	F(1)–Mn(a)–F(3)	91.1(1)
	2.102(1)		91.8(1)
Mn(a)–F(3)	1.816(2)	F(2)–Mn(a)–F(3)	92.4(1)
	1.808(2)		92.5(1)
Mn(c)–F(1)	2.128(3)	F(1)–Mn(c)–F(2)	91.5(1)
	2.134(2)		91.1(1)
Mn(c)–F(2)	1.913(2)	F(1)–Mn(c)–F(4)	92.2(1)
	1.910(1)		92.0(1)
Mn(c)–F(4)	1.806(2)	F(2)–Mn(c)–F(4)	91.0(1)
	1.806(2)		91.3(1)

$b = 7.6290(1)$ Å, $c = 5.7444(1)$ Å, $\beta = 90.402(2)°$ ($R_B = 4.5$, $R_P = 9.8$, $R_{WP} = 10.5$, $R_{EXP} = 7.3$ and $\chi^2 = 2.1$). The atomic coordinates are reported in table 1, selected atomic coordinates in table 2 and tilt angles around the three crystallographic axes in table 3. A [001] view of the unit cell is presented in figure 5 showing the antiferrodistortive ordering of the octahedra. It can be concluded that $KMnF_4$ and $RbMnF_4$ are isomorphic.

An interesting point is to verify how the BVS rule can predict some of the observed structural features in the $AMnF_4$ series. The BVS rule predicts in the absence of electronic and steric effects the following bond distances for $KMnF_4$ and $RbMnF_4$: Mn–F = 1.92 Å, K–F = 2.76 Å and Rb–F = 2.93 Å. Therefore, the unit cell parameter of the aristotype structure corresponding to $KMnF_4$ should be $a_{Mn-F} = 3.84$ Å, as calculated from the Mn–F distance, but $a_{K-F} = 3.19$ Å, as calculated from the K–F distance. In a similar way, the unit cell parameter of the aristotype structure corresponding to $RbMnF_4$ should be $a_{Mn-F} = 3.84$ Å

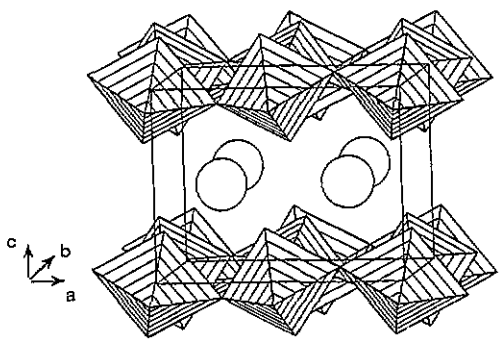

Figure 2. View of the unit cell of $RbMnF_4$ showing the layered character of this compound. $[MnF_2F_{4/2}]^-$ units are represented by octahedra and Rb atoms by open circles.

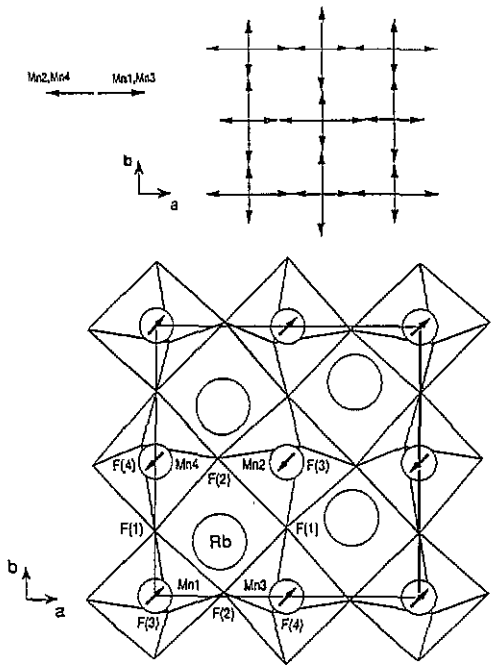

Figure 3. [001] view of the unit cell of $RbMnF_4$ showing the antiferrodistortive ordering of the octahedra and the orientation of the magnetic moments. The numbering of the spins refers to table 5.

but $a_{Rb-F} = 3.38$ Å. The epitaxy between the A cation and the MnF_4 layers requires the existence of a stress in the structure, proportional to $d_A = a_{Mn-F} - a_{A-F}$, which is partially relieved by tilting the octahedra. In this way, the atoms find new crystallographic positions minimizing d_A and satisfying, as well as possible, the BVS rule. Since $d_K > d_{Rb}$, the magnitude of the tilt angles should be more important for the K compound than for the Rb compound, as found experimentally (see table 3).

3.2. Magnetic study of $RbMnF_4$ and $KMnF_4$

In order to solve the magnetic structures of $RbMnF_4$ and $KMnF_4$ we have taken into account all the information about the symmetry and magnetic properties of these systems. To obtain a deeper insight into the nature of the magnetic couplings allowed by symmetry, a symmetry analysis of the possible magnetic structures has been performed. Since all the magnetic reflections can be indexed in the crystallographic unit cell, the propagation vector of the magnetic structure is $\boldsymbol{k} = (0, 0, 0)$. Using Bertaut's macroscopic theory (Bertaut 1968) we have obtained the irreducible representations of the space group $P2_1/a$ and the basis functions describing the possible magnetic structures (table 4). Taking into account the symmetry information, the magnetic structures of these two compounds were solved by trial and error. Due to the fact that the Mn atoms are in special positions, the magnetic structure factor can be easily written. Therefore, a rapid test as a function of the Miller indices of the most intense magnetic reflections can be performed by hand. This permits selection of the magnetic modes for each compound.

Table 3. Tilt angles (°) around each of the three crystallographic axes for $RbMnF_4$ and $KMnF_4$.[a]

a axis		*b* axis		*c* axis	
Mn(a) (0, 0, 0)	Mn(c) ($\frac{1}{2}$, 0, 0)	Mn(a) (0, 0, 0)	Mn(c) (0, $\frac{1}{2}$, 0)	Mn(a) (0, 0, 0)	Mn(c) (0, $\frac{1}{2}$, 0)
$RbMnF_4$ ($T = 9.6$ K)					
+17.82(8) [F(1)]	+16.68(7) [F(1)]	+13.76(8) [F(2)]	−15.14(8) [F(2)]	0.0(1) [F(1)]	0.0(1) [F(1)]
+15.7(1) [F(3)]	+15.2(1) [F(4)]	+12.66(8) [F(3)]	−13.49(8) [F(4)]	+3.38(5) [F(2)]	+3.72(6) [F(2)]
$KMnF_4$ ($T = 19.1$ K)					
+21.02(5) [F(1)]	+18.86(5) [F(1)]	+15.40(5) [F(2)]	−19.92(5) [F(2)]	0.0(1) [F(1)]	0.0(1) [F(1)]
+19.19(6) [F(3)]	+16.72(6) [F(4)]	+14.59(5) [F(3)]	−16.65(5) [F(4)]	+4.52(5) [F(2)]	+5.00(6) [F(2)]

[a] No correction has been made to take into account the influence of the distortion of the octahedra in the tilt angles. The fluorine atom used in the calculations is given in parentheses according to the labelling of table 1 and figures 3 and 5. See text for details.

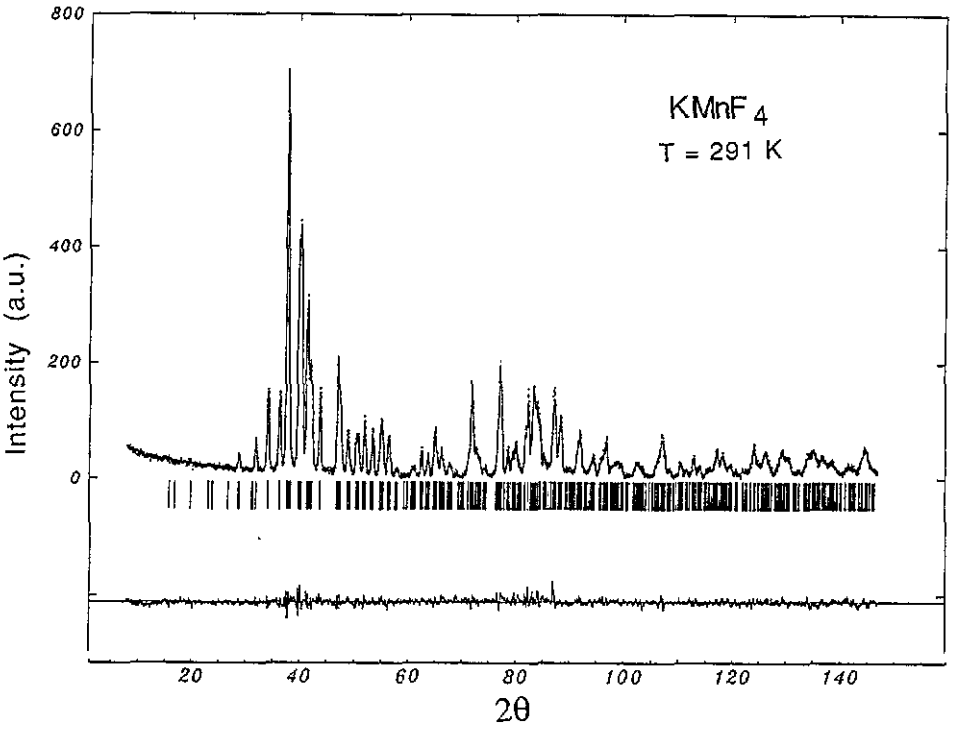

Figure 4. Observed (dotted curve), calculated (full curve) and difference neutron powder diffraction profiles for $KMnF_4$ at 291 K. The short vertical lines below the pattern represent the positions of the allowed Bragg reflections.

The fit of our experimental data to the different models by using the Rietveld method implemented in FULLPROF (Rodríguez-Carvajal 1990) shows unambiguously a collinear antiferromagnetic structure for $RbMnF_4$ and a non-collinear antiferromagnetic structure with four different sublattices for $KMnF_4$. In spite of the independence of the two Mn sites (a and c) we have performed the refinements with the constraints $|S(a)\mu| = |S(c)\mu|$ ($S\mu$ is the magnetic moment component, $\mu = x, y, z$) because the departure from orthorhombic symmetry is very small. It is worth remarking that the reported neutron powder diffraction experiments may not be sensitive enough to small canting angles between magnetic moments. Therefore, other experiments such as AC susceptibility measurements at zero external magnetic field would be required to verify the collinear antiferromagnetic ordering found for $RbMnF_4$.

The observed and calculated patterns at 1.5 K are presented in figure 6 for the K and Rb derivatives. The reliability factor R_M is 4.8 for $KMnF_4$ and 7.0 for $RbMnF_4$. Since the monoclinic crystal symmetry permits complete determination of the spin directions, the projection of the magnetic moment of each lattice along the three crystallographic axes has been obtained and is shown in table 5. The magnetic structure projected on the xy plane is presented in figures 3 and 5 for, respectively, the Rb and K derivatives. The angle between the two spin directions that the magnetic structure of $KMnF_4$ exhibits is 17° (see figure 5).

Concerning the symmetry analysis, the irreducible representation describing the magnetic structure of $KMnF_4$ is $\Gamma_{2g}(-)$ (table 4) being the coupling between the basis functions at the two Mn sites, Mn(a) and Mn(c), in anti-phase (table 5). On the other hand, the magnetic structure of $RbMnF_4$ is more complicated since the transition to the

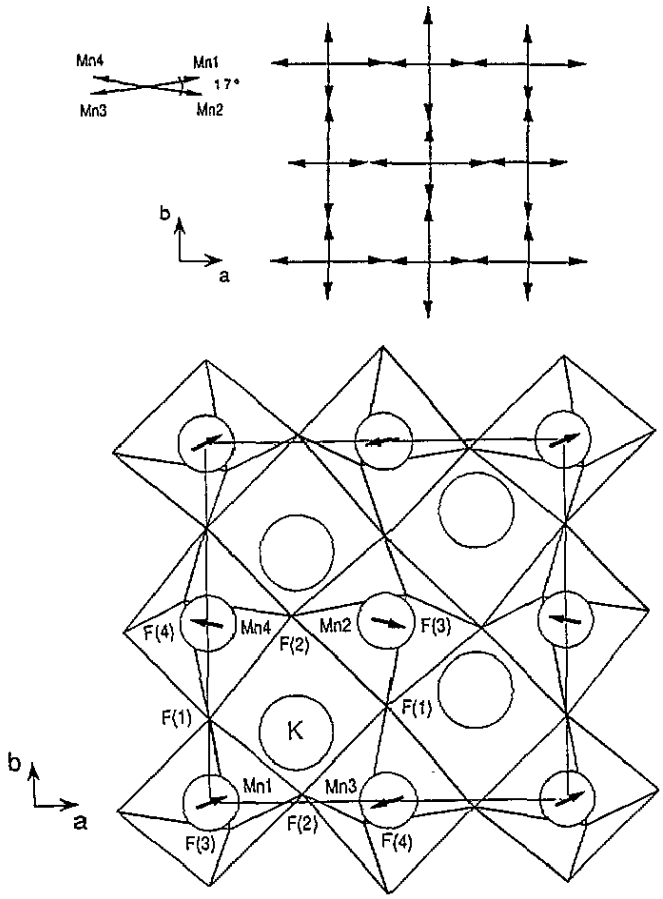

Figure 5. Projection of the unit cell of $KMnF_4$ along [001] showing the antiferrodistortive ordering of the octahedra and the orientation of the magnetic moments in the four magnetic sublattices. The numbering of the spins refers to table 5.

Table 4. Basis functions of the irreducible representations of the space group $P2_1/a$ for propagation vector $k = 0$ describing the possible magnetic structures for $RbMnF_4$ and $KMnF_4$. The magnetic modes are defined as $F = S_\alpha + S_\beta$ and $A = S_\alpha - S_\beta$ where S_i $(i = \alpha, \beta)$ is the spin (axial vector) of the sublattice i of a given Mn(a) or Mn(c) site. The relevant representations are even with respect to the symmetry centre and are labelled by the symbol Γ_g. In parentheses we give the character of the generator 2_{1y}.

Numbering of the Bravais sublattices corresponding to the sites Mn(a) and Mn(c)				
Mn(a):	(2a)	$\bar{1}$	(0, 0, 0):Mn1	$(\frac{1}{2}, \frac{1}{2}, 0)$:Mn2
Mn(c):	(2c)	$\bar{1}$	$(\frac{1}{2}, 0, 0)$:Mn3	$(0, \frac{1}{2}, 0)$:Mn4

Generators of $P2_1/a$: 2_{1y} $(\frac{1}{4}, y, 0)$ and $\bar{1}$ (0, 0, 0)

	Mn(a)			Mn(c)		
	x	y	z	x	y	z
$\Gamma_{1g}(+)$	A_x	F_y	A_z	A_x	F_y	A_z
$\Gamma_{2g}(-)$	F_x	A_y	F_z	F_x	A_y	F_z

magnetically ordered phase occurs following a mode which does not correspond to any basis function of either of the two irreducible representations (table 4). In fact this mode, $(A_x, A_y, A_z) = (A_x, 0, A_z) + (0, A_y, 0)$, can be written as the combination of the basis function of $\Gamma_{1g}(+)$ and $\Gamma_{2g}(-)$ with zero ferromagnetic components (see table 4) and

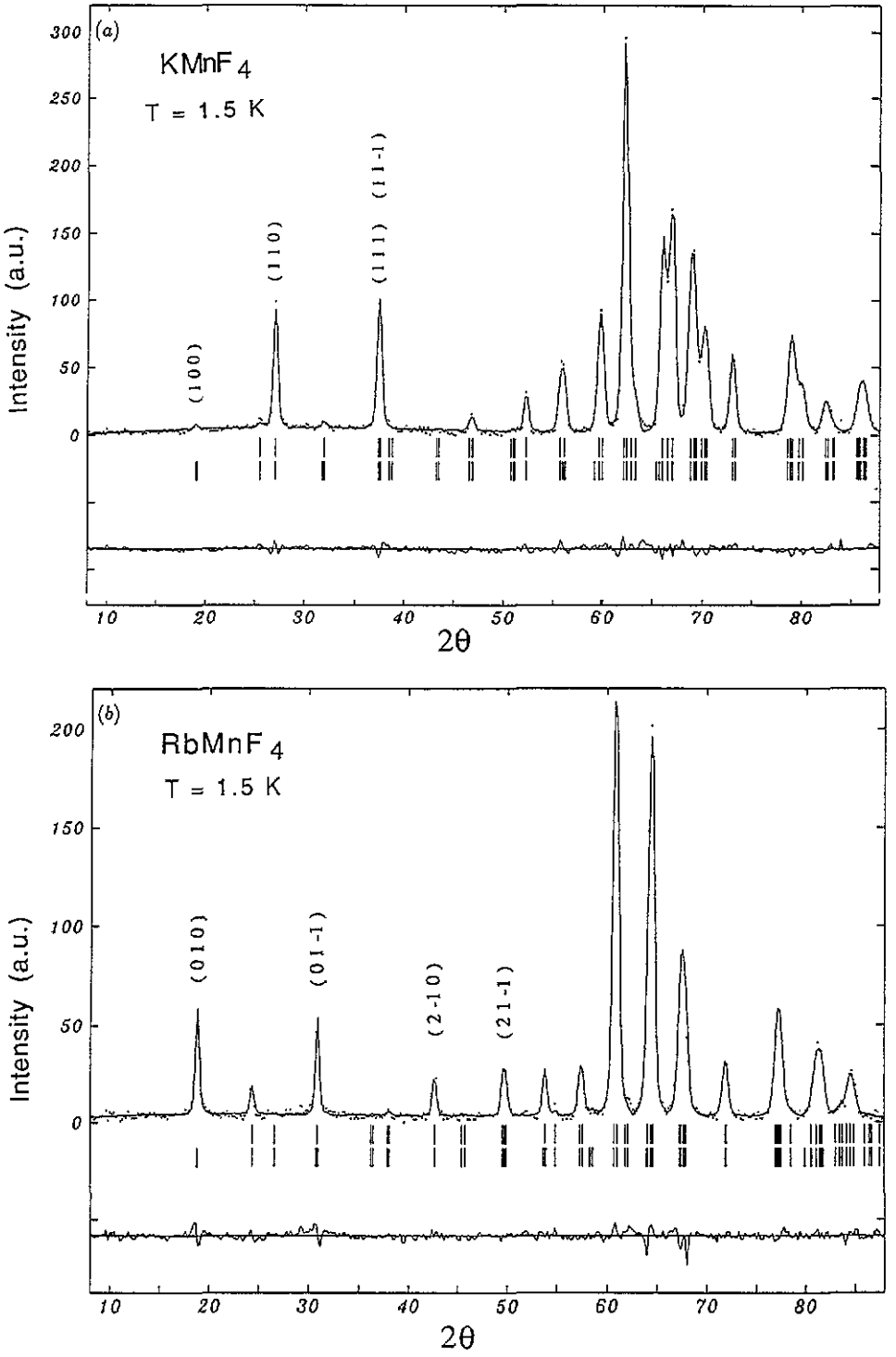

Figure 6. Observed (dotted curve) and calculated (full curve) nuclear and magnetic intensities at 1.5 K to (*a*) $KMnF_4$ and (*b*) $RbMnF_4$. The short vertical lines below the patterns represent the positions of the allowed Bragg reflections, the lower curve being the difference between the observed and calculated intensity at each step.

Table 5. Components of the magnetic moments (in Bohr magnetons) along the three crystallographic axes for $AMnF_4$ (A = Na, K, Rb, Cs).

	x	y	z	m_x	m_y	m_z	m (μ_B)
				$NaMnF_4$ [a] $T = 4$ K $k = (0, 0, \frac{1}{2})$			
Mn1	0	0	0	+2.7	−2.1	+1.0	3.5
Mn2	$\frac{1}{2}$	$\frac{1}{2}$	0	+2.7	−2.1	+1.0	
Mn3	$\frac{1}{2}$	0	0	−2.1	+2.7	−1.0	
Mn4	0	$\frac{1}{2}$	0	−2.1	+2.7	−1.0	
	$KMnF_4$ $T = 1.5$ K $k = (0, 0, 0)$ ($F_x^{(a)} - F_x^{(c)}$, $A_y^{(a)} - A_y^{(c)}$, $F_z^{(a)} - F_z^{(c)}$)						
Mn1	0	0	0	+2.55(4)	+0.42(7)	+1.18(7)	2.83(2)
Mn2	$\frac{1}{2}$	$\frac{1}{2}$	0	+	−	+	
Mn3	$\frac{1}{2}$	0	0	−	−	−	
Mn4	0	$\frac{1}{2}$	0	−	+	−	
	$RbMnF_4$ $T = 1.5$ K $k = (0, 0, 0)$ ($A_x^{(a)} + A_x^{(c)}$, $A_y^{(a)} + A_y^{(c)}$, $A_z^{(a)} + A_z^{(c)}$)						
Mn1	0	0	0	+1.97(4)	+1.97(4)	+1.03(9)	2.97(3)
Mn2	$\frac{1}{2}$	$\frac{1}{2}$	0	−	−	−	
Mn3	$\frac{1}{2}$	0	0	+	+	+	
Mn4	0	$\frac{1}{2}$	0	−	−	−	
				$CsMnF_4$ [b] $T = 2.2$ K $k = (0, 0, 0)$			
Mn1	0	0	0	+4.0(2)		0	4.0(2)
Mn2	$\frac{1}{2}$	$\frac{1}{2}$	0	+		0	
Mn3	$\frac{1}{2}$	0	0	+		0	
Mn4	0	$\frac{1}{2}$	0	+		0	

[a] Data from Molinier *et al* (1991). The unit cell from this reference has been transformed into a similar cell to that of the other compounds (see text). In the true monoclinic cell, Mn1 is equivalent to Mn2 and Mn3 to Mn4. The magnetic mode in this cell is (A_x, F_y, A_z) with m(Mn1) = (3.7, 0.4, 1.0). At variance with the rest of the compounds, the coupling between layers is antiferromagnetic.

[b] Data from Massa and Steiner (1980). The direction of the magnetic moments in the basal plane cannot be determined from powder data.

corresponds to a reducible representation of the direct sum $\Gamma_{1g}(+) \oplus \Gamma_{2g}(-)$. The mixture of the irreducible representations is an unusual feature exhibited by around 10% of the total number of magnetic structures for which a symmetry analysis has been performed (Izyumov *et al* 1979). In the case of the Rb derivative, the coupling between the basis functions at the two Mn sites is in phase (table 5).

D1B neutron powder diffractograms are depicted in figure 7 for $KMnF_4$ (ΔT = 1.5–9.4 K) and $RbMnF_4$ (ΔT = 1.5–4.8 K) in the angular range $8° \leqslant 2\theta \leqslant 88°$. The enhancement observed in some of the Bragg reflections corresponds to the magnetic ordering of the sample. The integrated intensities of three Bragg reflections with large magnetic contribution have been calculated from magnetic structure refinements and are shown in figure 8 as a function of the temperature. Moreover, the dependence on the temperature of the magnitude of the sublattice magnetic moment has been calculated by means of magnetic structure refinement. Figure 9 shows the temperature dependence of the sublattice magnetization for both K and Rb derivatives. From figures 8 and 9 it is possible to determine that magnetic ordering occurs below 5.2 ± 0.1 K and 3.7 ± 0.1 K for, respectively, $KMnF_4$ and $RbMnF_4$.

The magnetic moment of each sublattice at 1.5 K is $2.83(2)\mu_B$ and $2.97(3)\mu_B$ for the K and Rb derivatives, respectively. The expected value of the saturated magnetic moment for an Mn^{3+} ion with $S = 2$ is $4\mu_B$. There are several reasons to support the reduction of the observed magnetic moments. At 1.5 K (T_c = 5.2 and T_c = 3.7 for, respectively,

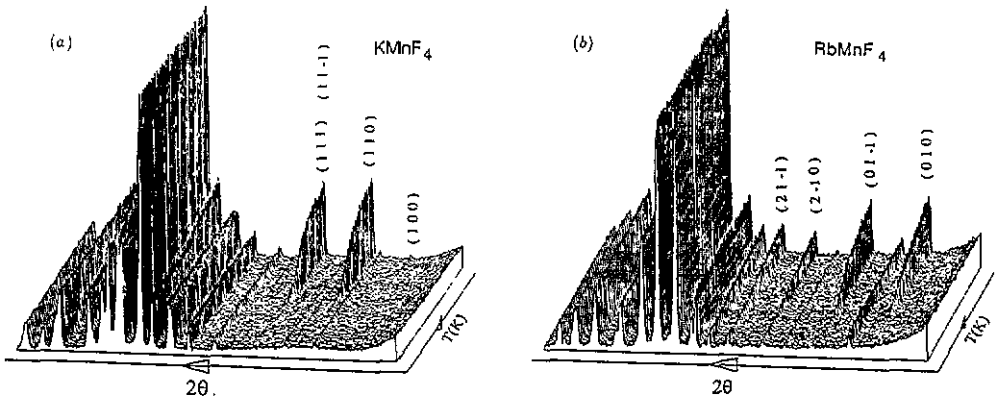

Figure 7. 3D plot of the neutron powder diffraction patterns as a function of the temperature in the range $8° \leqslant 2\theta \leqslant 88°$ for (*a*) $KMnF_4$ ($\Delta T = 1.5$–9.4 K) and (*b*) $RbMnF_4$ ($\Delta T = 1.5$–4.8 K). The index of the Bragg peaks showing strong magnetic contribution is depicted.

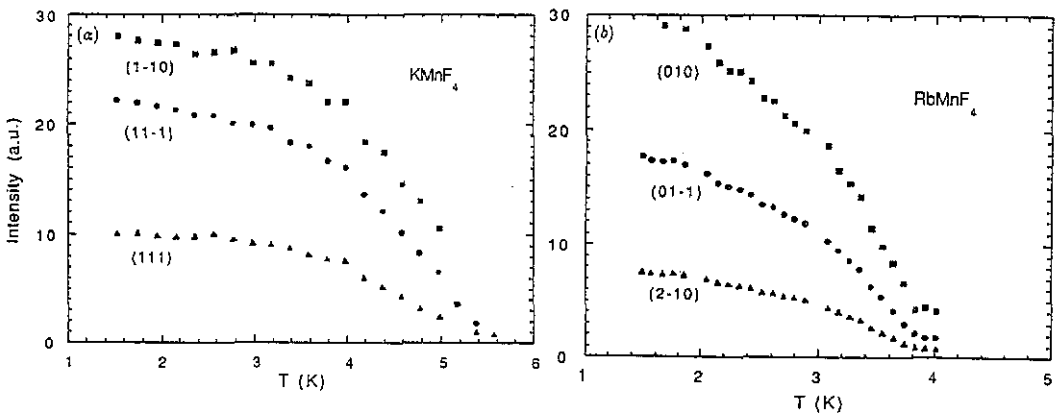

Figure 8. Integrated intensities of a series of Bragg reflections with large magnetic contribution as a function of the temperature. The data correspond to (*a*) $KMnF_4$ and (*b*) $RbMnF_4$.

the K and Rb derivatives) the magnetocrystalline anisotropy of the Mn^{3+} ions may not permit complete saturation of the magnetic moments. In addition, incomplete quenching of the orbital moment and the two-dimensional (2D) character of these two compounds can also contribute to the observed reduction of the magnetic moments. The zero-point spin reduction due to quantum fluctuations is much larger in 2D than in three-dimensional (3D) antiferromagnets (Lines 1967). Moreover, spin–orbit coupling splits the $^5B_{1g}$ ground state in two doublets and a singlet. In the case of $CsMnF_4 \cdot 2H_2O$ the excited doublet and singlet levels are at 7.9 K and 32.4 K, respectively, from the doublet ground state (Palacio and Morón 1993). A similar reduction in the value of the magnetic moment has also been reported for the related layered-perovskite Mn^{3+} fluoride $TlMnF_4$ which exhibits a magnetic moment of $3.1\mu_B$ at 1.3 K ($T_c = 4.2$ K) (Nuñez *et al* 1992).

The temperature dependence of the sublattice magnetization for $KMnF_4$ and $RbMnF_4$ shows only minor differences in the behaviour of both compounds (figure 9). In the critical region the sublattice magnetization is expected to vary as $M(T)/M(0) = B(1 - T/T_c)^{\beta}$. A log–log plot of $M(T)/M(1.5\text{ K})$ versus $1 - T/T_c$ (see inset in figure 9) yields a β

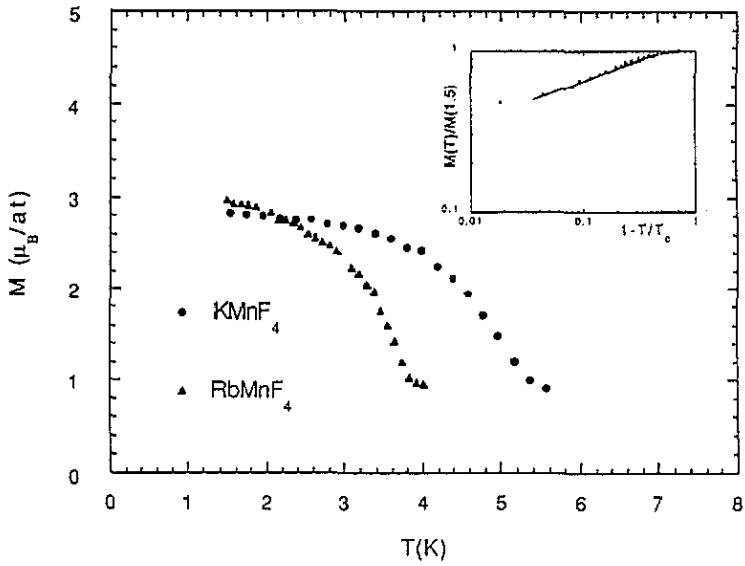

Figure 9. Temperature dependence of the magnetic moment of each sublattice for $KMnF_4$ (●) and $RbMnF_4$ (▲). The inset corresponds to a log–log plot of $M(T)/M(1.5\text{ K})$ versus $1-T/T_c$.

value of 0.26 and an amplitude of 1.20 for both compounds in the temperature range $0.03 < 1 - T/T_c < 0.3$. This plot indicates that both compounds belong to the same universality class.

The existence of spontaneous ordering in 2D systems is very sensitive to the spin symmetry. Thus, in the Ising model there is a conventional phase transition to an ordered state with $\beta = \frac{1}{8}$. In the XY model the Kosterlitz–Thouless phase transition yields a state of infinite correlation length with no spontaneous order (Kosterlitz and Thouless 1973). In the Heisenberg model there is no phase transition above 0 K; however, in real systems the presence of an interlayer exchange of only $10^{-4}J$ where J is the nearest-neighbour exchange, is sufficient to induce 3D order. The critical exponent β has an asymptotic value close to the 3D one of $\simeq \frac{1}{3}$ and it can be observed in a generally small temperature range. However, according to Bramwell and Holdsworth (1992), below T_c there is a crossover to a second regime of finite size 2D behaviour with a well defined β value of $3\pi^2/128 \simeq 0.23$. Monte Carlo simulations show that this second regime can be observed in the range $0.03 < 1 - T/T_c < 0.4$ (Bramwell and Holdsworth 1992). These values of β have been observed for a variety of quasi-ideal 2D compounds with planar anisotropy (e.g. K_2CuF_4, $\beta = 0.22$ (Hirakawa and Ikeda 1973); $Mn(HCO_2)_2{\cdot}2H_2O$, $\beta = 0.23$ (de Jongh and Miedema 1974); Gd_2CuO_4, $\beta = 0.23$ (Chattopadhyay *et al* 1992)).

Our experimental observations are also in good agreement with the above theoretical predictions. The critical regime extends over about the same reduced temperature region as found in the Monte Carlo calculations. The value of $\beta = 0.26$ is slightly higher than the theoretical one; however, similar values have been observed in other 2D systems possessing strong interlayer coupling, such as $RbFeF_4$, $\beta = 0.25$ (de Jongh and Miedema 1974); Rb_2CrCl_3Br and $Rb_2CrCl_2Br_2$, $\beta = 0.26$ (Hutchings *et al* to be published).

There are several experimental difficulties in extending the temperature range of $M(T)$ to values of $1 - T/T_c$ lower than 10^{-2}. Critical scattering is particularly important in lower-dimensional systems. It affects the intensity of the magnetic peaks in the proximities and at

both sides of the ordering temperature, since it peaks at T_c while magnetic Bragg scattering goes to zero at T_c. An additional difficulty is the uncertainty of T_c. Because of the layer nature of these compounds it may well be that the powder grains have a distribution of strain with a concomitant smearing of the critical temperature. Moreover, given the rather large samples used in the neutron diffraction experiments and the temperature control of the cryostat the sample temperature cannot be determined with an uncertainty smaller than 3% to the temperature region around T_c. Therefore, with the available experimental data it is not possible to extend the determination of the critical exponent β nearer to T_c and to observe the expected crossover to $\beta \simeq \frac{1}{3}$.

4. Discussion

In this section, the relationship between crystal structure and magnetic properties of the Rb and K derivatives is discussed in the framework of the $AMnF_4$ (A = Na, K, Rb, Cs) series. Moreover, the sign of the superexchange interaction and the origin of the canting between spins are also discussed.

The nuclear and magnetic structures of the K and Rb derivatives have already been examined in section 3. Both compounds are isomorphic, space group $P2_1/a$, and order as antiferromagnets. However, the magnetic moments are non-collinear in $KMnF_4$. The Na compound crystallizes in the space group $P2_1/a$ with $a = 5.760(2)$ Å, $b = 4.892(1)$ Å, $c = 5.755(2)$ Å, $\beta = 108.62(1)°$ and $Z = 2$ at 70 K (Molinier *et al* 1991). On the other hand, the crystal structure of $CsMnF_4$ has been refined in the space group $P4/n$ with $a = 7.9148(2)$ Å, $c = 6.3069(2)$ Å and $Z = 4$ at 24.3 K (Rodríguez–Carvajal *et al* to be published). There is only one Mn site in both compounds which is located at a symmetry point $\bar{1}$. As in the case of the K and Rb derivatives, the crystal structures of $NaMnF_4$ and $CsMnF_4$ consist of layers of $[MnF_2F_{4/2}]^-$ corner-sharing octahedra separated by the alkali ions. The octahedra are also distorted exhibiting three different Mn–F distances which are shown in table 6. The shortest Mn–F distance corresponds to the axial fluorine atoms, the long axis of the octahedra being antiferrodistortively ordered within the layers (figure 10). The increase of the separation between layers, which corresponds to the c unit cell parameter, is directly related to the increase of the size of the alkali ion within the $AMnF_4$ series (table 6).

Concerning the magnetic properties, $CsMnF_4$ has been described as a ferromagnet below 18.9 ± 0.5 K (Massa and Steiner 1980). The magnetic moments of this compound lie on the layers having a value of $4.0(2)\mu_B$ at 2.2 K. On the other hand, the monoclinic crystal symmetry of $NaMnF_4$ permits complete determination of the spin directions (Molinier *et al* 1991). The Na derivative orders as a non-collinear antiferromagnet below $T_c = 13.0 \pm 0.5$ K with a canting angle of 13° (figure 10). The components of the magnetic moment of each sublattice, $3.5\mu_B$ at 4 K, are referred to a transformed supercell ($\boldsymbol{a}' = \boldsymbol{a} + \boldsymbol{b}$, $\boldsymbol{b}' = -\boldsymbol{a} + \boldsymbol{b}$, $\boldsymbol{c}' = \boldsymbol{c}$) for easy comparison with the K, Rb and Cs compounds (table 5 and figure 10). It is worth mentioning that the magnetic structure of $NaMnF_4$ has a propagation vector $\boldsymbol{k} = (0, 0, \frac{1}{2})$. Thus, the magnetic cell is doubled along the c axis. It is also important to point out that, contrary to the other members of the $AMnF_4$ series ($\boldsymbol{k} = 0$), the superexchange interaction between consecutive layers is negative (antiferromagnetic) for the Na compound. The increase of the interlayer separation seems to favour the ferromagnetic coupling.

Mechanisms for the sign of the magnetic interaction between cation moments, via an anion intermediary, in an ionic crystal have been proposed and given semiquantitative

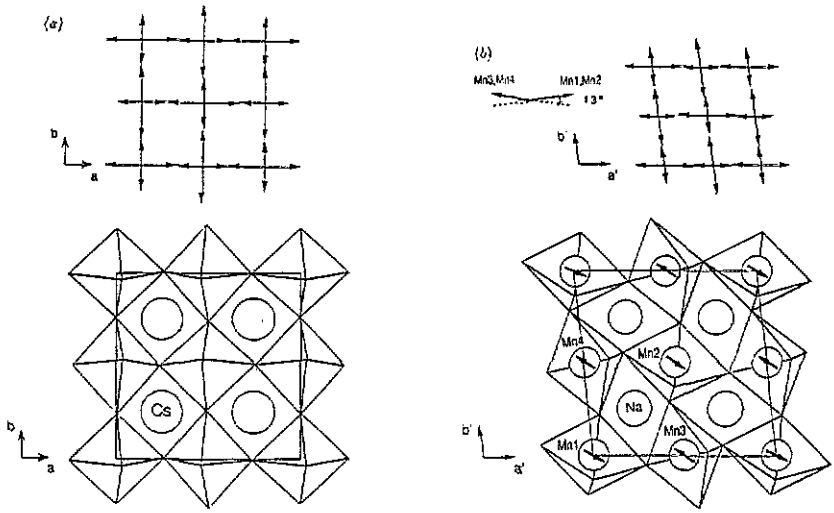

Figure 10. [001] view of the unit cell of (*a*) $CsMnF_4$ and (*b*) $NaMnF_4$ showing the antiferrodistortive ordering of the octahedra. The orientation of the magnetic moments for $NaMnF_4$ is shown referred to the supercell ($a'b'c'$) (see text). The numbering of the spins relates to table 5.

justification (Goodenough 1963, 1958, 1955, Kanamori 1959). These rules depend upon the number and configuration of the d electrons at the cations on both sides of the intermediary anion. Therefore, to properly apply these rules it is necessary to know the electron configuration of the cation. The outer-electron configuration is $3d^4$ for Mn^{3+} in the $AMnF_4$ series which yields a twofold degenerate E_g orbital ground state for cubic symmetry. Orbital degeneracy is removed because of the Jahn–Teller effect. This means that the cubic symmetry is not stable and the crystal field at the $3d^4$ cation is less symmetrical, as experimentally observed in the $AMnF_4$ series (table 6).

Van Vleck (1939) showed that the normal vibration modes that split the E_g levels are those illustrated in figure 11. Positive Q_3 stabilizes the d_{z^2} orbital, negative Q_3 stabilizes the $d_{x^2-y^2}$ orbital and Q_2 stabilizes a mixture of the two. Moreover, Kanamori (1960) has shown that the ratio Q_3/Q_2 that is present in a given static distortion is given by $\tan\phi = [(2/\sqrt{6})(2m - l - s)]/[\pm(2/\sqrt{2})(l - s)]$ where s, m and l are the short, medium and long cation–anion bond lengths of the distorted octahedra. If the static distortion is determined only by Q_3 (local tetragonal distortion) then $m = s$ and $\phi = 30°$, while if it is determined only by Q_2 then $2m = l + s$ and $\phi = 0°$ (Kanamori 1960). If $0° \leqslant \phi < 30°$, the distortion due to the pure Jahn–Teller effect is orthorhombic. If the local symmetry is lower, other effects are superimposed. These can be steric, which seem to be the present case, or electronic (strong spin–orbit coupling, for instance). It is noteworthy that steric effects are also responsible for the additional distortion that monoclinic perovskite MnF_3 exhibits. MnF_3 also shows three Mn–F distances: $l = 2.09$ Å, $m = 1.91$ Å and $s = 1.79$ Å (Hepworth and Jack 1957), which corresponds to $\phi = 6.6°$.

The essential factor in understanding magnetic coupling between $3d^4$ ions is that the electron ordering associated with the Q_3 mode gives completely empty orbitals directed along the s and m bonds and half-filled orbitals directed along the l bonds, while the electron ordering associated with the Q_2 mode gives electron density not only along the l bonds but also, although smaller, along the m bonds (Goodenough 1963). From the particular structural arrangement of the distorted $[MF_2F_{4/2}]^-$ octahedra within the $AMnF_4$

Table 6. Main structural and magnetic parameters concerning the magneto-structural correlations in the $AMnF_4$ series.

A	A radius (Å)	T (K)	c (Å)	Mn–F_{ax}(s) (Å)	Mn–F_{eq}(m) (Å)	Mn–F_{eq}(l) (Å)	ϕ[a] (°)	Mn–F_{eq}–Mn (°)	T_c (K)	J_{13}[b]	J_{14}[c]	Magnetic ordering	Canting angle (°)
Na[d]	1.18	70	5.755(1)	1.818(5)	1.860(6)	2.179(5)	23.9	138.4(3)	13.0 ± 0.5	–	–	NC-AF	13
K[e]	1.51	19.1	5.7444(1)	1.808(2)♠	1.923(2)♠	2.102(1)♠	7.2♠	146.4(1)△	5.2 ± 0.1	–	–	NC-AF	17
				1.806(2)◇	1.910(1)◇	2.134(2)◇	11.8◇	140.1(1)▽					
Rb[e]	1.61	9.6	5.9968(2)	1.802(3)♠	1.960(4)♠	2.108(3)♠	1.0♠	150.3(1)△	3.7 ± 0.1	+	–	C-AF	0
				1.824(3)◇	1.920(3)◇	2.094(4)◇	9.6◇	145.5(1)▽					
Cs[f]	1.74	24.3	6.3069(2)	1.816(2)	1.924(3)	2.095(2)	7.4	159.9(1)	18.9 ± 0.5	+	+	C-F	0

[a] The ratio Q_3/Q_2 that is present in a given Jahn–Teller static distortion (see text).

[b] Sign of the isotropic exchange interaction between adjacent octahedra along the a axis. These signs have been deduced from the magnetic structures in table 5 (see also figures 3, 5 and 10). We have considered that the overall spin arrangement is mainly due to isotropic exchange between nearest neighbours.

[c] Sign of the isotropic exchange interaction between adjacent octahedra along the b axis.

[d] Data from Molinier *et al* (1991).

[e] This work.

[f] Structural data from Rodríguez-Carvajal *et al* (to be published) and magnetic data from Massa and Steiner (1980).

♠: Mn(a) octahedron.

◇: Mn(c) octahedron.

△: along the a axis.

▽: along the b axis.

NC-AF: non-collinear antiferromagnet.

C-AF: collinear antiferromagnet.

C-F: collinear ferromagnet.

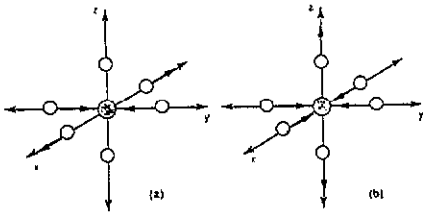

Figure 11. The normal vibration modes (*a*) Q_2 ($Q_2 > 0$) and (*b*) Q_3 ($Q_3 > 0$).

series it is possible to deduce the sign of the exchange interaction along the [100] and [010] directions by applying the Goodenough–Kanamori rules (Goodenough 1963, 1958, 1955, Kanamori 1959).

If a pure $Q_3 > 0$ mode happens on adjacent octahedra, which are antiferrodistortively ordered (...Mn–*l*–F–*s*–Mn...) and connected via an angle of 180°, ferromagnetic interaction takes place via pσ overlap of half-filled d_{z^2} (*l* bond) with empty (*s* bond) $d_{x^2-y^2}$ orbitals. Such an interaction weakens as the Mn–F–Mn angle decreases. The reason is an enhancement of the pπ overlap between adjacent half-filled t_{2g} orbitals which gives an antiferromagnetic contribution. A ferrodistortive ordering (...Mn–*l*–F–*l*–Mn...) should give strong (half-filled d_{z^2} – half-filled d_{z^2}) antiferromagnetic coupling along the *z* direction and weak (empty $d_{x^2-y^2}$ – empty $d_{x^2-y^2}$: ...Mn–*s*–F–*s*–Mn...) antiferromagnetic coupling along the orthogonal directions.

On the other hand, a pure Q_2 mode (or hybrid Q_3/Q_2) on adjacent octahedra can give either ferro- or antiferromagnetic coupling depending on the degree of orbital filling and the particular *l*, *m*, *s* spatial ordering. A well known example is the above-mentioned MnF_3 which exhibits antiferrodistortive *l*–*s* ordering in a basal plane (exchange angle $\simeq 148°$) and *m*–*m* ordering along the perpendicular direction (exchange angle $\simeq 144°$). Ferromagnetic coupling is observed in the basal plane and antiferromagnetic coupling is observed along the perpendicular direction (Wollan *et al* 1958).

The ϕ parameter together with the Mn–F–Mn angles and *l*, *m* and *s* bonds are shown in table 6 for each member of the series. The four compounds exhibit both Q_2 and Q_3 contributions, although the Q_3 contribution seems to be more important for the Na compound†. It is worth mentioning that, in all cases, we have antiferrodistortive ordering in the basal plane of *l* and *m* bonds, the *s* bond always being slightly canted from the *c* axis. This arrangement is not the same as that found in MnF_3 but we may still have ferromagnetic coupling within the basal plane if the superexchange angles Mn–F–Mn are near to 180°. From tables 5 and 6 it is clear that we can determine the value $\alpha \simeq 147°$ for the critical superexchange angle α_c at which the crossover between ferro- ($\alpha > \alpha_c$) and antiferromagnetic ($\alpha < \alpha_c$) isotropic interaction takes place in this series. This is nicely verified in the case of the Rb compound. $RbMnF_4$ closely follows the above prescription since its magnetic structure exhibits antiferromagnetic interaction along the *b* axis with $\alpha_{b\text{-axis}} < \alpha_c$ but ferromagnetic interaction along the *a* axis with $\alpha_{a\text{-axis}} > \alpha_c$ (see figure 3 and table 6).

An additional interesting result can be obtained from the comparison between T_c and the $\alpha - \alpha_c$ values for each member of the series. The isotropic magnetic interaction, which scales with the critical temperature, can be written to first-order approximation as $J(\alpha) \propto (\alpha - \alpha_c)$. This relation is clearly verified along the $AMnF_4$ series as can be deduced from the values

† We believe that the structural data concerning the Na compound should be considered with caution as they correspond to a powder refinement carried out from 6° to 86° at 2θ and $\lambda = 2.52$ Å (Molinier *et al* 1991). Therefore the F positions could not be accurate enough. If Na data from table 6 are correct, $NaMnF_4$ is the most 'anisotropic' (higher content of Q_3 mode) member of the $AMnF_4$ series.

of T_c and α listed in table 6 for each member of the series. Thus, the lowest (highest) T_c is exhibited by the Rb (Cs) derivative since it is this compound which presents the lowest (highest) value for the $\alpha - \alpha_c$ parameter.

Another point to be considered is the relationship between canting angle and magnetic anisotropy in this family of compounds. The most common spin–spin interactions found in insulating systems are of superexchange and dipolar types. The effects of the magnetic dipole–dipole interaction are generally negligible except at very low temperatures. Isotropic superexchange interaction does not impose any particular direction of the magnetic moments with respect to the crystal frame. This interaction tends just to keep the spins exactly parallel or antiparallel depending on its sign. Except in cases of topological frustration or competition between nearest- and next-nearest-neighbour interactions, the pure isotropic exchange interaction gives collinear magnetic structures. Therefore, anisotropic terms are required in order to explain non-collinear structures.

Single-ion anisotropy at inequivalent lattice sites as well as antisymmetric exchange interaction, which is anisotropic in character, are two possible causes of spin canting (Moriya 1960a, b). An important source of magnetic anisotropy in octahedral Mn^{3+} compounds is the distortion of the octahedra due to the Jahn–Teller effect (Palacio *et al* 1991). When the orientation of adjacent octahedra is very different, as happens in the $AMnF_4 \cdot H_2O$ series, single-ion anisotropy can compete with isotropic exchange to give non-collinear structures. Then, it seem that this interaction does not play an important role in the case of the $AMnF_4$ series. More probably the antisymmetric Dzyaloshinsky–Moriya term of the general exchange Hamiltonian, $\boldsymbol{D}_{ij}\ (\boldsymbol{S}_i \times \boldsymbol{S}_j)$, is the agent of the spin canting observed in the Na and K compounds. The reason for this can be found in the collinear structures observed for Rb and Cs. The departure from tetragonal symmetry is very small in these two compounds and, therefore, $\boldsymbol{D} \simeq 0$. Moreover, the anisotropic (symmetric) exchange has a strength proportional to $(\Delta g/g)^2 J$, which is weaker than $D \simeq (\Delta g/g) J$, where g is the gyromagnetic ratio and Δg its departure from the free electron value ($g = 2$).

5. Concluding remarks

The crystal structures of $KMnF_4$ and $RbMnF_4$ are strongly influenced by the size of the alkali ions and the cooperative Jahn–Teller effect. The overall crystal symmetry is mainly governed by steric effects as may be seen by the deviation from tetragonal symmetry as the size of the alkali ion diminishes.

The crystal structure largely influences the magnetic properties of the $AMnF_4$ series. It is worth stressing the fact that the weak superexchange interaction between layers changes its sign between Na (negative) and K (positive). A nice verification of the $J(\alpha) \propto (\alpha - \alpha_c)$ relation and the qualitative Goodenough–Kanamori rules for the sign of the isotropic exchange interaction has been shown, the example of $RbMnF_4$ being particularly illustrative. Anisotropic terms are required in order to explain the non-collinear magnetic structures exhibited by $NaMnF_4$ and $KMnF_4$. The antisymmetric Dzyaloshinsky–Moriya term of the general exchange Hamiltonian seems to be the origin of the spin canting observed in these two compounds.

A more detailed and quantitative study of the second-order effects due to anisotropic interactions together with AC susceptibility and magnetization measurements are in progress.

Acknowledgments

We thank S T Bramwell, P C W Holdsworth and D Visser for helpful discussions concerning the values of the critical exponents and for kindly providing us with results prior their publication. We are also gratefully indebted to Professor J L Fourquet. The research in Zaragoza has been supported by grants MAT88-0174 and MAT/91-681 from the Comisión Interministerial de Ciencia y Tecnología.

References

Aleksandrov K S, Beznosikov B V and Misyul S V 1987 *Ferroelectrics* **73** 201–20
Bertaut E F 1968 *Acta Crystallogr.* A **24** 217–31
Bramwell S T and Holdsworth P C W 1992 *37th Ann. Conf. on Magnetism and Magnetic Materials (Houston, TX)*
—— 1993 *J. Appl. Phys.* at press
Brese N E and O'Keeffe M 1991 *Acta Crystallogr.* B **47** 192–7
Brown I D and Altermat D 1985 *Acta Crystallogr.* B **41** 244–7
Chattopadhyay T, Brown P J, Stepanov A A, Zvyagin A I, Barilo S N and Zhigunov D I 1992 *J. Magn. Magn. Mater.* **104-107** 607–8
de Jongh L J and Miedema A R 1974 *Adv. Phys.* **23** 1–260
Goodenough J B 1955 *Phys. Rev.* **100** 564–73
—— 1958 *J. Phys. Chem. Solids* **6** 287–97
—— 1963 *Magnetism and the Chemical Bond* (New York: Wiley)
Hepworth M A and Jack K H 1957 *Acta Crystallogr.* **10** 345–51
Hirakawa K and Ikeda H 1973 *J. Phys. Soc. Japan* **35** 1328–36
Hutchings M T, Als Nielsen J, Bramwell S T and Visser D to be published
Izyumov Y A, Naish V E and Petrov S B 1979 *J. Magn. Magn. Mater.* **13** 275–82
Kanamori J 1959 *J. Phys. Chem. solids* **10** 87–98
—— 1960 *J. Appl. Phys. Suppl.* **31** 14–23S
Kaucic V and Bukovec P 1979 *J. Chem. Soc. (Dalton Trans.)* 1512–5
Köhler P, Massa W, Reinen D, Hofmann B and Hoppe R 1978 *Z. Anorg. (Allg.) Chem.* **446** 131–58
Kosterlitz J M and Thouless D J 1973 *J. Phys. C: Solid State Phys.* **6** 1181–203
Lines M E 1967 *Phys. Rev.* **164** 736–48
Massa W and Steiner M 1980 *J. Solid State Chem.* **32** 137–43
Molinier M, Massa W, Khairoun S, Tressaud A and Soubeyroux J L 1991 *Z. Naturf.* B **46** 1669–73
Moriya T 1960 *Phys. Rev.* **117** 635–47, **120** 91–8
Morón M C, Bulou A, Pique C and Fourquet J L 1990 *J. Phys.: Condens. Matter* **2** 8269–75
Morón M C, Palacio F and Rodríguez-Carvajal J 1992 *Physica* B **180 & 181** 125–7
Nuñez P, Tressaud A, Grannec J, Hagenmuller P, Massa W, Babel D, Boireau A and Soubeyroux J L 1992 *Z. Anorg. (Allg.) Chem.* **609** 71–6
Palacio F, Andrés M, Esteban-Calderón C, Martínez-Ripoll M and García-Blanco S 1988 *J. Solid State Chem.* **76** 33–9
Palacio F, Andrés M, Rodríguez-Carvajal J and Pannetier J 1991 *J. Phys.: Condens. Matter* **3** 2379–90
Palacio F and Morón M C 1993 *Research Frontiers in Magnetochemistry* ed C O'Connor (Singapore: World Scientific)
Pebler J, Massa W, Lass H and Ziegler B 1987 *J. Solid State Chem.* **71** 87–94
Rodríguez-Carvajal J 1990 *Satellite Meeting on Powder Diffraction (XVth Conf. Int. Union of Crystallography (Toulouse, 1990))* p 127
Rodríguez-Carvajal J, Palacio F and Morón M C to be published
Van Vleck J H 1939 *J. Chem. Phys.* **7** 72–84
Wandner K H and Hoppe R 1987 *Z. Anorg. (Allg.) Chem.* **546** 113–21
Wollan E O, Child H R, Khoeler W C and Wilkinson M K 1958 *Phys. Rev.* **112** 1132–6